

# Airflow basin structure numerical optimisation analysis and suction nozzle characteristics experimental study of vacuum-vibration tray precision seeder

Caiqi Liao, Jin Chen, Fanzhao Geng, Xueming Tang

College of Mechanical Engineering, Jiangsu University, Zhenjiang, Jiangsu, China

## Abstract

The stable and uniformly distributed airflow field can effectively improve the seed suction effect and seed-carrying stability of the pneumatic seeder. With this end in view, this paper optimised the airflow basin structure of the vacuum-vibration tray precision seeder based on the computational fluid dynamics (CFD) simulation technology. The results show that the airflow field is relatively stable and well-distributed when the chamber height is 50 mm, and the outlet tube diameter is 65 mm. In addition, the thickness of the base plate with suction holes should be less than 5 mm, and the needle suction nozzle guide should be greater than 15 mm, according to the numerical analysis results. Based on the above study, the seeding characteristics of the needle-type suction nozzle and the plate-type suction nozzle were further explored to determine the type of nozzle more suitable for a rectangular sucker. Through various experimental designs, the significant influencing factors of the two suction nozzles, their appropriate working ranges, and the optimal combination of working parameters were determined in turn. The needle suction nozzle requires a lower suction height and less grain dispersion, according to the experi-

mental results, while the plate suction nozzle is just the opposite; it allows a certain suction height to be maintained with the seeds and requires high dispersion of grain. In general, the plate suction nozzle can obtain better seeding performance and is a more favourable nozzle for the vacuum-vibration tray precision seeder.

## Introduction

With the improvement of the seeding qualified rate and seedling success rate of rice factory seedlings, vacuum precision seeding devices are widely used and occupy a large market in domestic and international agricultural mechanised planting (Yasir & Liao, 2014). As 'Fine Agriculture' advances, higher demands are being placed on traditional seeding equipment, so improving the performance of suction precision seeders to meet the growing agricultural demand is essential.

Many researchers have been working to improve the seeding performance of the seeding device by exploring suitable operating parameters. Gaikwad and Sirohi (2008) fabricated a low-cost pneumatic seeder and experimentally determined that the optimum suction pressure for picking capsicum and tomato seeds was 4.91 kPa and 3.92 kPa, respectively. Zhao *et al.* (2018) analysed the effect of the seed layer thickness on the seeding effect of the vacuum-vibration tray precision seeder through a two-phase flow coupling simulation technique and found that the suitable seed layer thickness was 15 to 25 mm. Liao *et al.* (2019) analysed the working principle of the tube-needle centralised seeding device. They obtained the optimal working parameter range of American ginseng seeding by optimising the regression model of the seed metering shaft speed, positive pressure, and negative pressure. Interestingly, numerous studies have pointed out that the right pneumatic state is crucial for obtaining high-quality seeding performance. In the field trials of a low-cost seedling tray seeder for lettuce, Tiw-An *et al.* (2020) found that the vacuum level dramatically influenced the seeding effectiveness of the device. Increasing the vacuum pressure was found to be an effective way to improve the seed suction capacity of the tray seeder by Liu *et al.* (2010), and similar experimental results were also found in Xia *et al.* (2008) and Hassan and Liao (2014).

The pneumatic conditions directly influence the seeding effect, and the air chamber, as the main air basin structure of the vacuum-vibration tray precision seeder, to a great extent, determines the overall uniformity and stability of the airflow field. Therefore, the most fundamental way to improve the seeding performance of the vacuum precision seeder is to optimise the air basin structure. By replacing the plates with different numbers of holes in the bench tests, Yazgi and Degirmencioglu (2014) determined that the best seeding performances for cotton and corn were obtained respectively when the plate with 26 holes and 36 holes were used. Gaikwad and Sirohi (2008) used the same method to determine the optimum suction nozzle size for adsorbing cap-

Correspondence: Jin Chen, College of Mechanical Engineering, Jiangsu University, Zhenjiang, Jiangsu, 212013, China.  
E-mail: chenjinjd126@126.com ; 542343600@qq.com

Key words: Computational fluid dynamics simulation; experimental design; seeding characteristics; structural optimisation; vacuum-vibration tray precision seeder.

Funding: this paper was fully supported by the National Natural Science Foundation of China [grant number 31871528].

Received for publication: 15 October 2021.

Accepted for publication: 28 June 2022.

©Copyright: the Author(s), 2022

Licensee PAGEPress, Italy

Journal of Agricultural Engineering 2022; LIII:1294

doi:10.4081/jae.2022.1294

This article is distributed under the terms of the Creative Commons Attribution Noncommercial License (by-nc 4.0) which permits any non-commercial use, distribution, and reproduction in any medium, provided the original author(s) and source are credited.

Publisher's note: All claims expressed in this article are solely those of the authors and do not necessarily represent those of their affiliated organizations, or those of the publisher, the editors and the reviewers. Any product that may be evaluated in this article or claim that may be made by its manufacturer is not guaranteed or endorsed by the publisher.

sicum and tomato seeds, respectively. In recent years, computational fluid dynamics (CFD) technology has developed rapidly and has become the mainstream method for optimising the airflow domain structure of the air-suction seeder. Gao and Zhang (2016) found in the Fluent simulation results that the lowest air losses could be achieved by using the 90° smooth circular elbow to connect the air chamber, which provides sound advice for the pipe structure design of the 2BQM-2 air suction planter. Through the hydrodynamics principles and fluent simulation numerical analysis, Du *et al.* (2017) determined that the sucker suction performance is more stable when there are two suction ports on the seed sucker. Based on the CFD technology, Liu *et al.* (2020) determined that the optimum transverse duct diameter of the wheat uniform seeding mechanism is 8 mm and the optimum negative pressure port diameter is 36 mm, and then developed a prototype accordingly, which could achieve good sowing results.

In order to improve the seeding performance of a vacuum-vibration tray precision seeder, this paper explores the appropriate size of a rectangular sucker that can obtain the most stable and uniform airflow field based on CFD techniques. In addition, the seeding characteristics and performance of the needle type and the plate type nozzles are compared in field trials to determine the optimum nozzle structure more suitable for the vacuum-vibration tray precision seeder.

## Materials and methods

### Computational fluid dynamics simulations

#### Generation of the air basin mesh

According to the actual size of the sucker, a three-dimensional airflow basin model was established, and the 10 mm computational domain was extended at the air inlet to ensure the stability of the airflow. The unstructured tetrahedral mesh was used to delineate the whole fluid domain. In addition, the local encryption operation was applied to the mesh of the suction holes to ensure the accuracy of the numerical calculation. The final fluid domain meshing effect is shown in Figure 1. The mesh qualities calculated according to the aspect ratio of the tetra elements are all above 0.3.

#### Boundary conditions and solution parameter settings

The mesh model was imported into Fluent 19.2, and the SIMPLE coupling solver was used to solve for the aerodynamic state of it. The airflow in the sucker is in a turbulent state. The velocity of the airflow within the air chamber is much less than the speed

of sound, and therefore the airflow in the sucker can be considered incompressible. According to the Boussinesq assumptions, the continuity equation and Reynolds equation (Krishnasreni, 2004) for the mean flow of the airflow are given in Eqs. 1 and 2, respectively.

$$\frac{\partial \rho}{\partial t} + \frac{\partial(\rho u_i)}{\partial x} = 0 \tag{1}$$

$$\frac{\partial(\rho u_i)}{\partial t} + \frac{\partial(\rho u_i u_j)}{\partial x_i} = \frac{\partial p}{\partial x_i} + \frac{\partial}{\partial x_j} \left( \mu \frac{\partial u_i}{\partial x_j} - \overline{\rho u_i u_j} \right) + S_i \tag{2}$$

$\rho$ , fluid density, kg/m<sup>3</sup>;  $u_i, u_j (i, j = 1, 2, 3)$ , the mean of speed, m/s;  $p$ , the mean of pressure, Pa;  $\mu$ , turbulent viscosity coefficient, Pa·s;  $\overline{\rho u_i u_j}$  -Reynolds stress term (Versteeg & Malalasekera, 1995);  $S_i$ , source term.

Eqs. 1 and 2 are not closed, so new turbulence models must be introduced. In this paper, the standard  $k - \epsilon$  model is used, introducing a transport equation of turbulent kinetic energy  $k$  and an equation about the turbulent dissipation rate  $\epsilon$ . The corresponding transportation equations (Wang, 2004) are shown in Eqs. 3 and 4. Eqs. 1-4 are the governing equations for solving the fluid state in the fluid domain:

$$\frac{\partial(\rho k)}{\partial t} + \frac{\partial(\rho k u_i)}{\partial x_i} = \frac{\partial}{\partial x_j} \left[ \left( \mu + \frac{\mu_t}{\sigma_k} \right) \frac{\partial k}{\partial x_j} \right] + G_k + G_b - \rho \epsilon - Y_M + S_k \tag{3}$$

$$\frac{\partial(\rho \epsilon)}{\partial t} + \frac{\partial(\rho \epsilon u_i)}{\partial x_i} = \frac{\partial}{\partial x_j} \left[ \left( \mu + \frac{\mu_t}{\sigma_\epsilon} \right) \frac{\partial \epsilon}{\partial x_j} \right] + C_{1\epsilon} \frac{\epsilon}{k} (G_k + C_{3\epsilon} G_b) - C_{2\epsilon} \rho \frac{\epsilon^2}{k} + S_\epsilon \tag{4}$$

In Eqs. 3 and 4, there are:

$$G_k = \mu_t \left( \frac{\partial u_i}{\partial x_j} + \frac{\partial u_j}{\partial x_i} \right) \frac{\partial u_i}{\partial x_j}; G_b = \beta g_i \frac{\mu_t}{Pr_t} \frac{\partial T}{\partial x_i}; Y_M = 2 \rho \epsilon Ma^2 \tag{5}$$

$G_k$ , generation term of the turbulent kinetic energy  $k$  caused by average velocity gradient;  $G_b$ , generation term of the turbulent kinetic energy  $k$  caused by buoyancy;  $Y_M$ , contribution of pulsation expansion in compressible turbulence;  $Pr_t$ , turbulent Prandtl number;  $\beta$ , coefficient of the thermal expansion;  $C_{1\epsilon}, C_{2\epsilon}, C_{3\epsilon}$ , empirical constant;  $S_k, S_\epsilon$ , source term;  $Ma$ , Mach number.

The inlet face of the airflow domain model was set to the pressure-inlet condition with an initial pressure value of 0 Pa. The outlet face was set to the pressure-outlet condition with an initial pressure

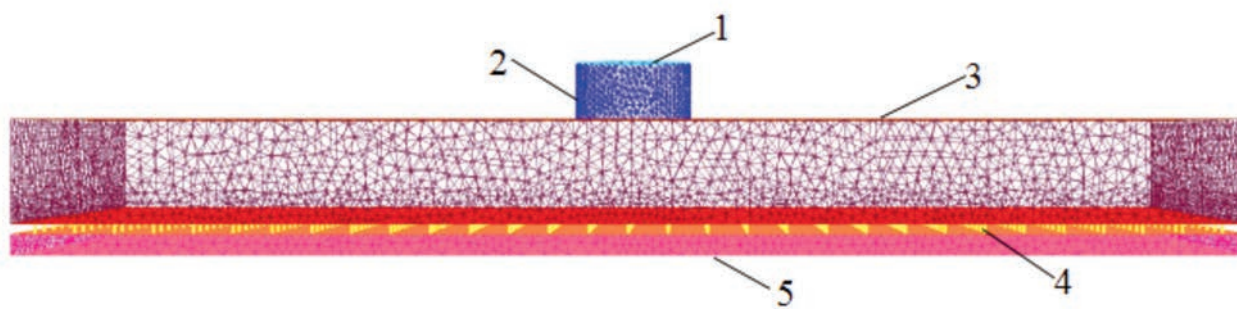


Figure 1. Schematic diagram of grid division of air chamber: 1. outlet face; 2. outlet tube; 3. rectangular chamber shell; 4. inlet face; 5. suction holes.

value of  $-15$  kPa. All other faces were set to the wall surface. After 300 iterations, the residuals of all varies were below 0.001, and the iterative convergence residual diagram is shown in Figure 2.

### Analysis of pneumatic losses on the sucker

The flow of fluid along the air basin structure results in a certain amount of energy loss, which can be divided into two categories: fractional loss and minor loss (Han and Wang, 2016), according to whether the cross-section through which the fluid flows varies. According to the airflow basin structure of the sucker (Figure 3), abrupt changes in the structure of the air basin at the junction of the suction hole and the air chamber, and the air chamber and the outlet tube, will mainly generate minor losses. However, when air flows through the air chamber and suction holes, the size and direction of the airflow through the cross-section remain the same, and the fractional losses will be mainly generated.

According to the Darcy-Weisbach formula (Bernardi *et al.*, 2018), the fractional loss  $h_f$  is calculated as shown in Eq. 6.

$$h_f = \lambda \frac{l \cdot V^2}{d \cdot 2g} \quad (6)$$

$l$ , the length of the pipe, m;  $V$ , the mean velocity of the pipe section for the fluid flowing, m/s;  $d$ , the pipe diameter, m;  $\lambda$ , the resistance loss coefficient along the pipeline.

As the airflow in the sucker is in a turbulent state, the pipe roughness has little effect on the flow resistance, and the formula for calculating the resistance loss coefficient along the pipeline  $\lambda$  can be calculated by Eq. 7 (Han and Wang, 2016).

$$\frac{1}{\sqrt{\lambda}} = 2.1 \lg(Re\sqrt{\lambda}) - 0.8 \quad (7)$$

The calculation formula of the Reynolds coefficient  $Re$  is  $\frac{\rho V d}{\mu}$ , and  $\mu$  is hydrodynamic viscosity, Pa·s. Based on the empirical formula,  $\lambda = \frac{0.3164}{Re^{0.25}}$ .

Then, the fractional loss calculation formula on the sucker can be updated to Eq. (8).

$$h_f = \frac{791l\mu^{\frac{1}{4}}V^{\frac{7}{4}}}{2500gd^{\frac{5}{4}}\rho^{\frac{1}{4}}} \quad (8)$$

Eq. 8 shows that the fractional loss increases with the increase of the pipe length; this suggests that the suction guide and chamber height should be as short as possible for major fractional loss along the way. However, a certain length of pipe is usually required to develop and stabilise the airflow adequately, so the chamber height and suction hole guide need to be explored further. According to the Bordas formula (Liu *et al.*, 2020), the equations for minor losses in the sudden expansion and sudden contraction structure are given in Eqs. 9 and 10, respectively.

$$h_{j1} = \left(1 - \frac{A_1}{A_2}\right)^2 \frac{v_1^2}{2g} \quad (9)$$

$$h_{j2} = 0.5 \left(1 - \frac{A_2}{A_1}\right) \frac{v_2^2}{2g} \quad (10)$$

In where:  $h_{j1}$ ,  $h_{j2}$  are the minor losses of sudden expansion structure and sudden contraction structure, respectively.  $A_1$ ,  $A_2$  are the cross-sectional areas on both sides of the abrupt pipe, respectively, and  $v_1$ ,  $v_2$  indicate the air velocity of the corresponding section. From Eqs. 9 and 10, it can be seen that the minor losses are related to the ratio of the cross-sectional area of the abrupt structure. For the two abrupt structures of the sucker (Figure 3), the cross-sectional area of the air chamber is known, so selecting the suitable diameter of the suction holes and outlet tube is beneficial to reduce energy losses. However, because the diameter of the suction hole is usually determined by the shape and size of the seed, the diameter of the outlet tube needs further exploration, as with the chamber height and the suction hole guide.

## Results and discussion

### Simulation numerical analysis results

#### The effect of air chamber height on airflow state

The numerical simulations for air chamber models with the heights of 50 mm, 100 mm, 150 mm, and 200 mm were carried out, and the airflow conditions at the suction holes of the sucker bottom plate were recorded in Table 1. The higher average air

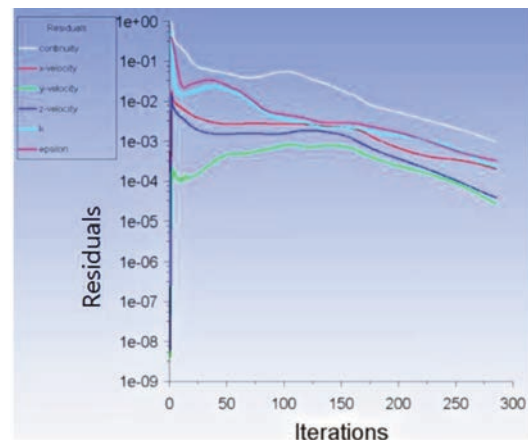


Figure 2. The iterative convergence residual diagram. The curves from top to down in the figure correspond to the continuity equation, the momentum equation in three directions, the turbulent kinetic energy equation, and the turbulent kinetic energy dissipation rate equation, respectively.

Table 1. Airflow state at suction holes with different chamber heights.

| Evaluation indexes                       | Air chamber heights (mm) |        |        |        |
|--|--------------------------|--------|--------|--------|
|  | 50                       | 100    | 150    | 200    |
| Average air velocity (m/s)               | 117.31                   | 113.80 | 110.43 | 111.35 |
| Standard deviation of air velocity (m/s) | 2.35                     | 1.80   | 6.30   | 2.54   |
| Average turbulent kinetic energy (J/kg)  | 440.26                   | 478.32 | 453.77 | 364.86 |

velocity at the suction holes means less fluid energy loss, and the lower standard deviation of the air velocity at each suction hole means better air distribution uniformity. In addition, the average turbulent kinetic energy at the suction holes was also given in Table 1, which can directly reflect the intensity of the turbulence.

In Table 1, the average air velocity at the suction holes decreased with the increase in chamber height but increased slightly at the chamber height of 200 mm. On the other hand, the standard deviation of air velocity at the suction holes did not vary significantly with the chamber height, with the worst uniformity of airflow distribution at the chamber height of 150 mm. Moreover, the average turbulent kinetic energy data increased first and then decreased. All the above phenomena could be explained by the fluid streamline diagram within the air chamber (Figure 4).

The air flowed into the air chamber through the suction holes and formed vortexes near the bottom plate due to the sudden widening of the airflow basin. At the chamber height of 50 mm (Figure 4A), the narrow spacing between the upper and lower plates of the chamber allowed the vortexes to flow more regularly in the chamber, and the streamlines within the chamber exhibited a high consistency even at the corners. As the chamber height increased, the fractional losses generated at the chamber height increased, so the average airflow velocity somewhat decreased. At the same time, the airflow was affected by corner conditions, making the airflow distribution within the chamber less uniform, and even secondary vortexes formed in the model with a chamber height of 150 mm. When the chamber height reached 200 mm (Figure 4D), the airflow was fully developed and could gently pass through the corners, effectively improving the average air velocity and airflow stability at the suction holes. Overall, the optimum average air velocity and good uniformity of airflow distribution can be achieved with a chamber height of 50 mm.

#### The effect of outlet tube diameter on airflow state

The airflow in the sucker was simulated for the outlet tube diameter of 25 mm, 45 mm, 65 mm, and 85 mm, respectively. The results are shown in Table 2.

As seen from Figure 5, the smaller the outlet tube diameter, the greater the difference in airflow velocity between the outlet tube and the air chamber. Furthermore, according to the minor loss equation (Eq. 10), the energy losses in the air chamber increased as the outlet tube diameter decreased and, accordingly, the average air velocity at the suction holes in Table 2 gradually decreased. Finally, the outlet tube diameter of 65 mm was determined to be a suitable choice for obtaining good velocity, distribution uniformity, and airflow stability.

#### The effect of suction hole guide on airflow state

Currently, the needle-type and plate-type suction nozzles are the two standard nozzle configurations for tray seeders (Zhao *et al.*, 2015), and their differences are mainly reflected in the suction

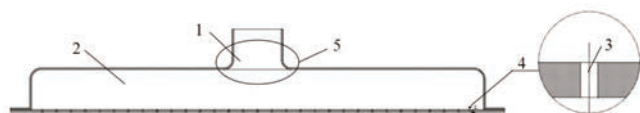


Figure 3. Airflow basin structure of sucker: 1. outlet tube; 2. air chamber; 3. suction hole; 4. sudden expansion structure; 5. sudden contraction structure.

hole guide. Then the effect of the suction hole guide on the airflow at the suction holes was investigated under the optimal chamber parameters determined from the above optimisation analysis. As shown in Figure 6, the airflow velocity tended to decrease as the

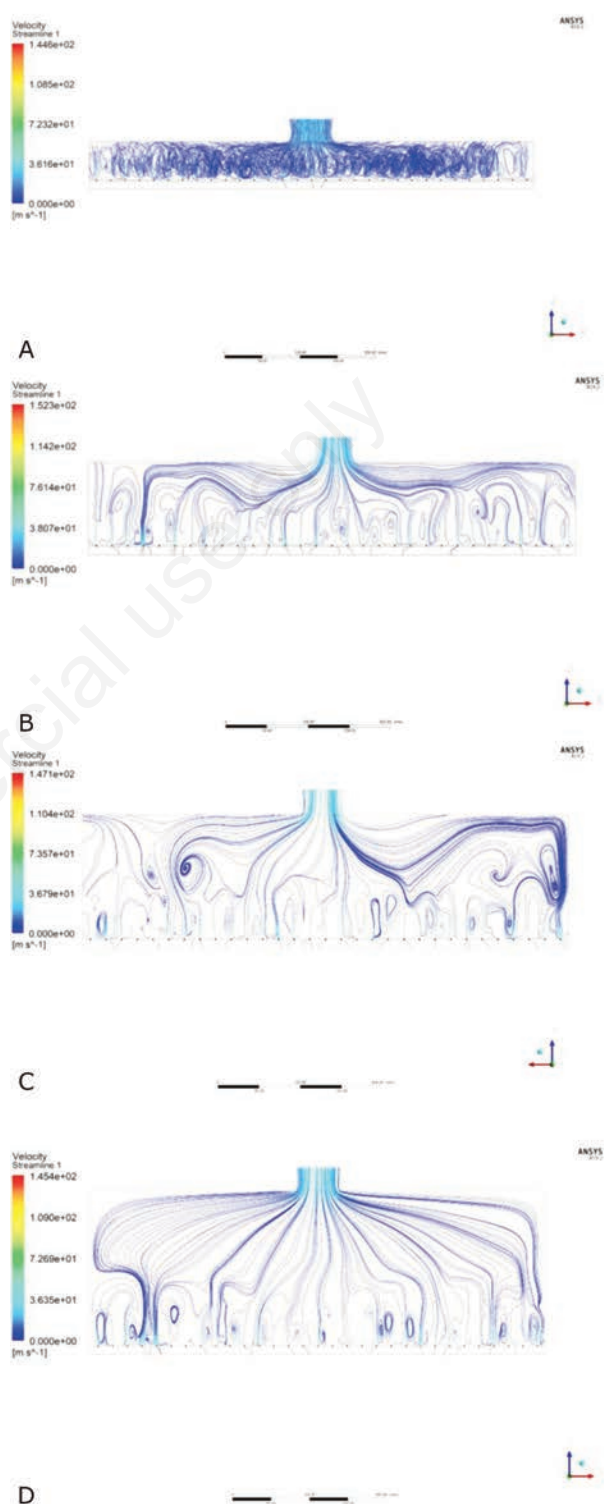


Figure 4. Streamline distribution with different chamber heights: A) With the chamber height of 50 mm; B) with the chamber height of 100 mm; C) with the chamber height of 150 mm; D) with the chamber height of 200 mm.

guide of the suction holes increased, which was consistent with the theoretical energy loss analysis. However, the air velocity rose after a sharp decline between the suction hole guide of 5 mm and 10 mm; this is because the airflow stabilized with the availability of sufficient airflow path. What is more, the air velocity standard deviation also improved when the suction hole guide exceeded 15 mm. Combining the simulation results and the actual constructional characteristics of the two types of nozzles, it can be concluded that the thickness of the base plate for plate-type suction nozzle should be less than 5 mm, which can obtain stronger pneumatic conditions. Moreover, the needle suction nozzle length should be greater than 15 mm, as the airflow stability is better. However, CFD numerical simulation analysis can only provide a reference for determining the guide of the two suction nozzles, and their seeding characteristics need to be further explored on the bench tests.

### Suction nozzle characteristics experimental study of vacuum-vibration tray precision seeder

A new sucker with a chamber height of 50 mm and an outlet tube diameter of 65 mm was customised according to numerical analysis results, and bench tests were carried out. The difference between the two nozzles is whether the bottom plate of the sucker is fitted with the plastic needles; the thickness of the bottom plate was 2 mm, the length of the plastic needle was 25 mm, and both types of nozzles with the suction hole diameter of 1 mm. The specification of the seedling tray used in the trials was 14×31 holes, and Suken 118 seeds were used in the trials.

#### Field test methods

##### Plackett-Burman design method

Several factors impact the seeding performance of vacuum-vibration tray precision seeders, but only a few make outstanding contributions. The Plackett-Burman (PB) experimental design method was used to comprehensively investigate seven common factors (Liu *et al.*, 2016; Montgomery, 2019; Zhao *et al.*, 2018) to quickly screen out the main factors. The elected factors and their symbols are given in Tables 3 and 4, all with two levels: high level (+1) and low level (-1). The PB experimental design with 12 experiments was selected, and the results were analysed in Design Export 10.0.

##### Steepest ascent method

The response surface models can reflect the true situation well when testing adjacent areas. This paper used the steepest ascent method to approximate the appropriate range of operating parameters to establish the more effective response surface equations.

##### Central composite design

In order to obtain the optimal working combination of seeder with different nozzles and to develop the empirical models between their respective seeding performance and significant factors, the Box-Behnken central composite design tests (Gunst *et al.*,

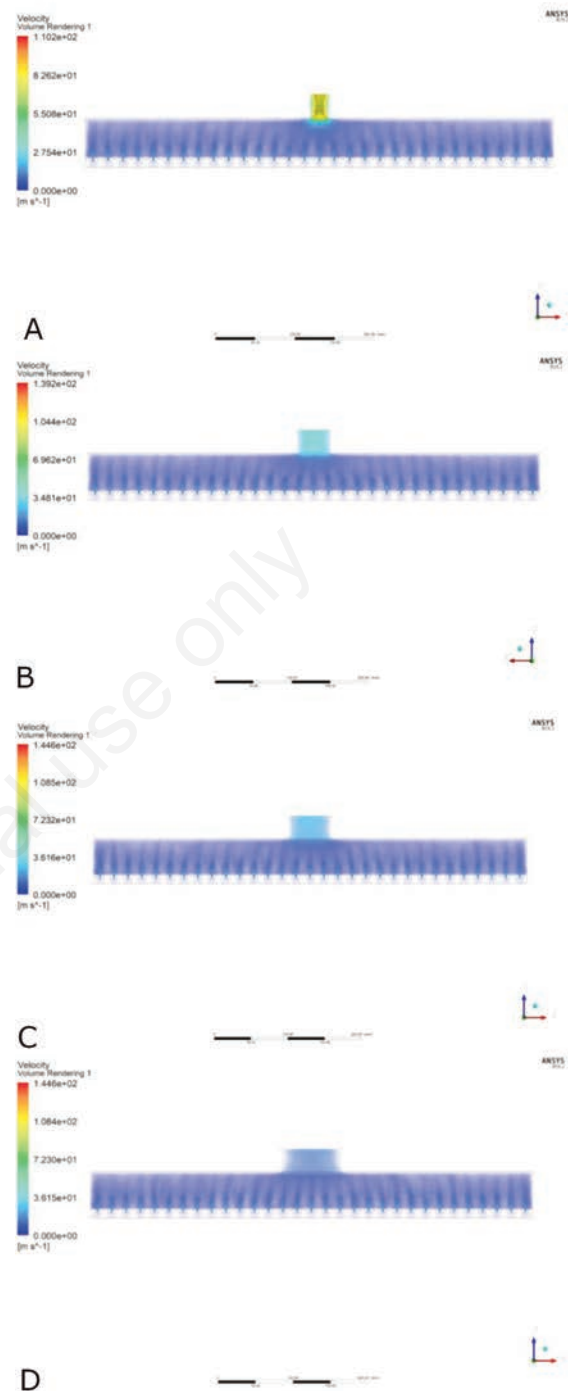


Figure 5. Air velocity distribution with different outlet tube diameters: A) with the outlet tube diameter of 25 mm; B) with the outlet tube diameter of 45 mm; C) with the outlet tube diameter of 65 mm; D) with the outlet tube diameter of 65 mm.

Table 2. Airflow state at suction holes with different outlet tube diameters.

| Evaluation indexes                       | Outlet tube diameters (mm) |        |        |        |
|--|----------------------------|--------|--------|--------|
|  | 25                         | 45     | 65     | 85     |
| Average air velocity (m/s)               | 89.91                      | 114.28 | 117.31 | 118.12 |
| Standard deviation of air velocity (m/s) | 1.91                       | 2.56   | 2.35   | 2.69   |
| Average turbulent kinetic energy (J/kg)  | 288.76                     | 423.93 | 440.26 | 449.89 |

1996) were designed based on the foregoing experiments. In this section, the values of the best combination of parameters identified in the steepest ascend experiments were used as the central level of each factor, and the single seed rate, over-seeding rate, and miss-seeding rate were employed as the evaluation indexes.

**Field test results and discussion**

**Analysis of Plackett-Burman experimental design results**

The PB experimental design analysis results are given in Table 4. The T values reflect the importance and effect of each influencing factor, and the P value shows the significance of the factors. Therefore, it can be seen that the vacuum, vibration frequency, and the seed suction height were the significant factors for both needle and plate suction nozzle with the P values all less than 0.05, but the order of importance and the influence effect of each influencing factors were different for the two nozzles.

For the needle-type suction nozzle, significant factors in order of importance were seed suction height > vibration frequency > vacuum and vibration frequency, seed suction height as well as vibration amplitude has a negative effect on seeding performance, while the vacuum has a positive effect. The order of importance for the plate suction nozzle was vacuum > vibration frequency > seed suction height, and all these significant factors show a positive effect.

Then the equations for the single seed rate of the needle-type and the plate-type nozzles in terms of actual factors were shown as Eqs. 11 and 12, respectively.

$$Y_N = 91.8 + 0.26A - 0.49B - 0.28C + 0.10D - 0.97E + 0.53F + G \quad (11)$$

$$Y_P = 79.77 + 0.34A + 0.41B + 0.22C + 0.06D + 0.65E + 0.97F - 1.38G \quad (12)$$

$Y_N$ , linear equation between single grain rate of needle suction nozzle and each affecting factor;  $Y_P$ , linear equation between single grain rate of plate suction nozzle and each affecting factor.

**Table 4. Plackett-Burman experimental analysis results.**

| Factors | Needle-type nozzle |         |            | Plate-type suction hole |         |            |
|---------|--------------------|---------|------------|-------------------------|---------|------------|
|         | T value            | P value | Importance | T value                 | P value | Importance |
| A       | 3.67               | 0.0215  | 3          | 4.80                    | 0.0087  | 1          |
| B       | -2.60              | 0.0599  | 4          | 2.19                    | 0.0935  | 4          |
| C       | -3.90              | 0.0175  | 2          | 3.14                    | 0.0349  | 2          |
| D       | 1.77               | 0.1507  | 5          | 1.01                    | 0.3709  | 7          |
| E       | -4.14              | 0.0144  | 1          | 2.78                    | 0.0496  | 3          |
| F       | 0.95               | 0.3977  | 7          | 1.72                    | 0.1610  | 6          |
| G       | 1.42               | 0.2289  | 6          | -1.95                   | 0.1223  | 5          |

**Table 5. Needle-type nozzle test results of steepest ascent path.**

| Group | Vacuum | Vibration frequency | Suction height | N-SSR |
|-------|--------|---------------------|----------------|-------|
| 1     | 18     | 12                  | 3              | 91.5  |
| 2     | 19     | 11                  | 2.5            | 92.8  |
| 3     | 20     | 10                  | 2              | 94.2  |
| 4     | 21     | 9                   | 1.5            | 93.5  |
| 5     | 22     | 8                   | 1              | 92.8  |

\*Single seed rate of needle-type nozzle.

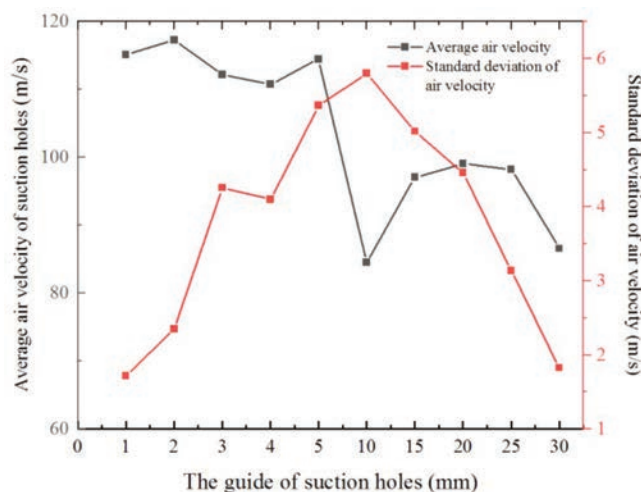


**Figure 6. The changing trend of airflow state with different guides of the suction holes.**

**Table 3. Factors and levels of Plackett-Burman design.**

| Symbols | Factors                      | Levels |     |
|---------|------------------------------|--------|-----|
|         |                              | -1     | +1  |
| A       | Vacuum (kPa)                 | 16     | 20  |
| B       | Vibration amplitude (mm)     | 3      | 4.5 |
| C       | Vibration frequency (Hz)     | 8      | 12  |
| D       | Seed thickness (mm)          | 10     | 15  |
| E       | Seed suction height (mm)     | 2.4    | 3.6 |
| F       | Inlet nozzle diameter (mm)   | 1      | 1.5 |
| G       | Residence time of suction(s) | 0.8    | 1.2 |

### Results analysis of the steepest ascent method

The steepest ascent method was used to approach the suitable working ranges of vacuum, vibration frequency, and seed suction height for the two nozzles. According to the estimated coefficient of Eqs. 11 and 12, the test programme was arranged by determining the gradient and direction of variation of each factor (Gunst *et al.*, 1996). The positive effect factors shall arrange in increasing order, and the negative effect factors shall arrange in decreasing order. The steepest ascent test scheme and results of needle type and plate type nozzles were shown in Tables 5 and 6, respectively.

The third group held the highest single seed rate in the tests of two suction nozzles. So, the levels of group 3 were taken as the central values for each parameter in the response surface designs.

### Response surface design results and analysis

The Box-Behnken central composite designs were carried out

on needle-type and plate-type suction nozzles, respectively; the variable levels are shown in Table 7, and the design schemes and results are recorded in Table 8. Based on the experimental results, the regression models of the single seed rate for the two nozzles were developed with the vacuum, vibration frequency, and suction height as the independent variables (Table 9). The analysis of variance for the needle and plate suction nozzle in Table 10 indicated that the established regression models were significant and can well reflect actual values with the P values of 0.0001 and 0.0009, respectively, and the adjusted coefficients of determination of 0.9717 and 0.9509.

Observing the single seed rate response surface of the needle-type suction nozzle (Figure 7), there was a clear interaction between the vibration frequency and the seed suction height within the set working parameter (Figure 7C). As can be seen from Figure 7A and B, when the vibration frequency and seed suction height

**Table 6. Plate-type nozzle test results of steepest ascent path.**

| Group | Vacuum | Vibration frequency | Suction height | P-SSR* |
|-------|--------|---------------------|----------------|--------|
| 1     | 18     | 11                  | 3.2            | 92.2   |
| 2     | 19     | 11.5                | 3.4            | 93.7   |
| 3     | 20     | 12                  | 3.6            | 95.2   |
| 4     | 21     | 12.5                | 3.8            | 94.0   |
| 5     | 22     | 13                  | 4.5            | 93.1   |

\*Single seed rate of plate-type nozzle.

**Table 7. Design factors and levels of Box-Behnken central composite test.**

| Symbols | Factors                  | Needle suction nozzle level |    |     | Plate suction nozzle level |     |      |
|---------|--------------------------|-----------------------------|----|-----|----------------------------|-----|------|
|         |                          | -1                          | 0  | 1   | -1                         | 0   | 1    |
| $X_1$   | Vacuum (kPa)             | 19                          | 20 | 21  | 19                         | 20  | 21   |
| $X_2$   | Vibration frequency (Hz) | 9                           | 10 | 11  | 11.5                       | 12  | 12.5 |
| $X_3$   | Suction height (mm)      | 1.5                         | 2  | 2.5 | 3.4                        | 3.6 | 3.8  |

**Table 8. Results of Box-Behnken central composite design.**

| Number | $X_1$ | $X_2$ | $X_3$ | Needle type |                  |                  | Plate type |     |     |
|--------|-------|-------|-------|-------------|------------------|------------------|------------|-----|-----|
|        |       |       |       | SSR*        | OSR <sup>o</sup> | MSR <sup>#</sup> | SSR        | OSR | MSR |
| 1      | -1    | -1    | 0     | 93.2        | 3.4              | 3.4              | 93.8       | 4   | 2.2 |
| 2      | 1     | -1    | 0     | 93.7        | 4                | 2.3              | 94.2       | 4.1 | 1.7 |
| 3      | -1    | 1     | 0     | 93.1        | 3.8              | 3.1              | 93.7       | 4.4 | 1.9 |
| 4      | 1     | 1     | 0     | 93.6        | 4.2              | 2.2              | 94         | 4.5 | 1.5 |
| 5      | -1    | 0     | -1    | 93.3        | 4.3              | 2.4              | 94.3       | 4.2 | 1.5 |
| 6      | 1     | 0     | -1    | 93.9        | 4.6              | 1.5              | 94.5       | 4.3 | 1.2 |
| 7      | -1    | 0     | 1     | 93.1        | 3.8              | 3.1              | 94.3       | 3.7 | 2   |
| 8      | 1     | 0     | 1     | 93.4        | 4.2              | 2.4              | 94.7       | 4   | 1.3 |
| 9      | 0     | -1    | -1    | 93.6        | 3.9              | 2.5              | 94.5       | 4.1 | 1.4 |
| 10     | 0     | 1     | -1    | 92.8        | 3.6              | 3.6              | 93.9       | 3.8 | 2.3 |
| 11     | 0     | -1    | 1     | 92.6        | 3.3              | 4.1              | 93.6       | 3.6 | 2.8 |
| 12     | 0     | 1     | 1     | 93.5        | 3.7              | 2.8              | 94.2       | 4.2 | 1.6 |
| 13     | 0     | 0     | 0     | 94.2        | 3.6              | 2.2              | 94.9       | 3.7 | 1.4 |
| 14     | 0     | 0     | 0     | 94.5        | 3.7              | 1.8              | 95.2       | 3.5 | 1.3 |
| 15     | 0     | 0     | 0     | 94.2        | 3.7              | 2.1              | 95.2       | 3.4 | 1.4 |
| 16     | 0     | 0     | 0     | 94.1        | 3.9              | 2                | 95         | 3.7 | 1.3 |
| 17     | 0     | 0     | 0     | 94.4        | 3.5              | 2.1              | 95.4       | 3.5 | 1.1 |

\*Single seed rate; <sup>o</sup>over-seeding rate; <sup>#</sup>miss-seeding rate.

are constant, the single seed rate increases with the vacuum, but there is a slight decline near 21 kPa as the over-seeding rate is increased at this moment. Similar findings were shown on the response surface of the plate suction nozzle (Figure 8). In Figure 8A, the slope of the surface of the single seed rate with vibration frequency was steeper than that of the vacuum, indicating that the

vibration frequency has a more significant impact on the single seed rate.

The best combination of working parameters for the two nozzles can be obtained by optimising their regression models. When the vacuum was 20.4 kPa, the vibration frequency was 9.9 Hz, and the seed suction height was 1.9 mm, the single seed rate of the nee-

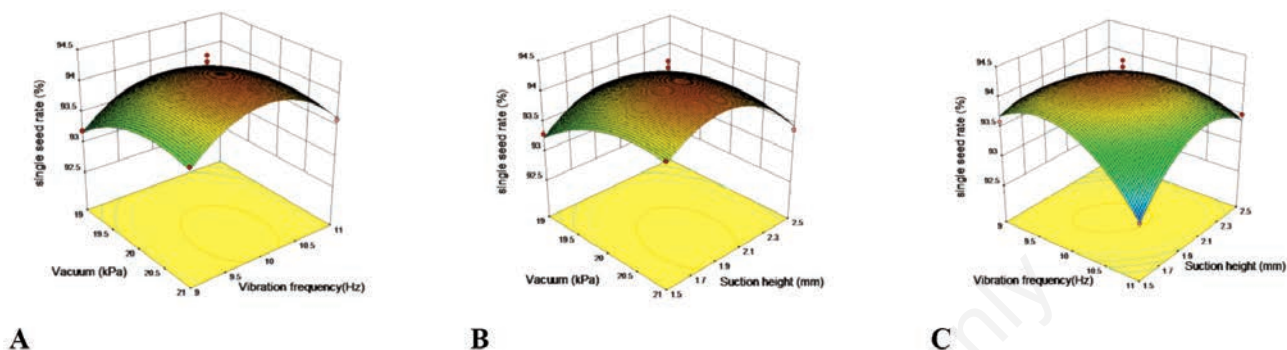


Figure 7. Response surface of interactive factors on single seed rate of needle suction nozzle. A)  $Y_{1SSR} = f_N(X_1, X_2, 0)$ ; B)  $Y_{1SSR} = f_N(X_1, 0, X_3)$ ; C)  $Y_{1SSR} = f_N(0, X_2, X_3)$ .

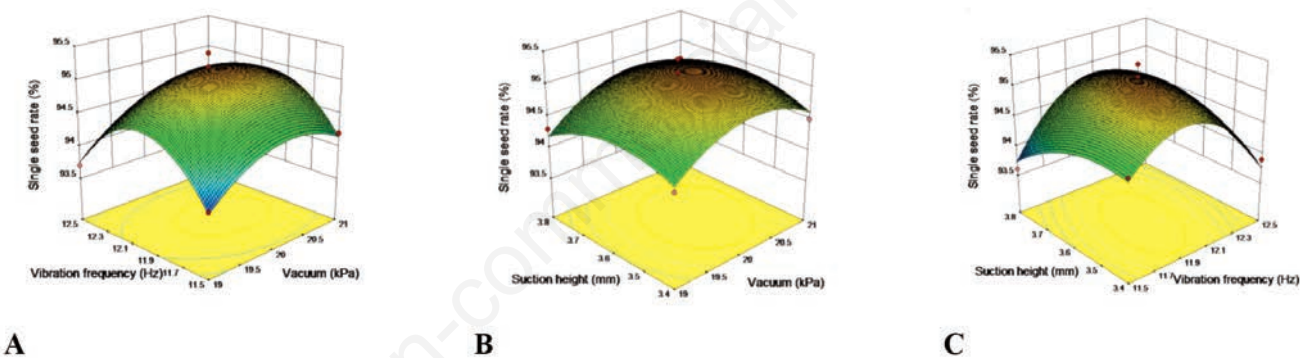


Figure 8. Response surface of interactive factors on single seed rate of plate suction nozzle. A)  $Y_{2SSR} = f_P(X_1, X_2, 0)$ ; B)  $Y_{2SSR} = f_P(X_1, 0, X_3)$ ; C)  $Y_{2SSR} = f_P(0, X_2, X_3)$ .

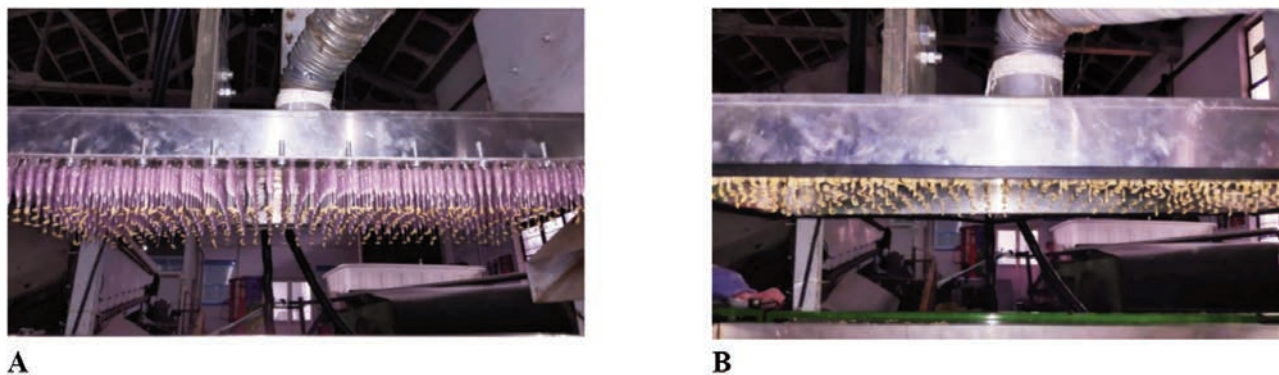


Figure 9. Seed-sucking effects of needle and plate suction nozzle. A) Seed-sucking effect of needle suction nozzle; B) Seed-sucking effect of plate suction nozzle.

**Table 9. Needle and plate suction nozzle single seed rate models.**

| Model | Fitting equation  | r <sup>2</sup> | Adj r <sup>2</sup> |
|-------|---|----------------|--------------------|
| 1     | $f_N = -82.885 + 12.1375X_1 + 10.0875X_2 + 3.29X_3 - 0.15X_1X_3 + 0.85X_2X_3 - 0.29X_3 - 0.59X_2^2 - 2.26X_3^2$               | 0.9717         | 0.9353             |
| 2     | $f_P = -490.36 + 16.1625X_1 + 67.645X_2 + 9.6X_3 - 0.05X_1X_2 + 0.25X_1X_3 + 3X_2X_3 - 0.4075X_1^2 - 3.23X_2^2 - 7.0625X_3^2$ | 0.9509         | 0.8878             |

**Table 10. Variance analysis of needle and plate suction nozzle single seed rate model.**

| Sources                       | Adj SS   | f <sub>N</sub> <sup>*</sup><br>F value | P-value | Adj SS   | f <sub>P</sub> <sup>o</sup><br>F value | P-value |
|-------------------------------|----------|--|---------|----------|--|---------|
| Model                         | 4.82     | 26.68                                  | 0.0001  | 4.73     | 15.06                                  | 0.0009  |
| X <sub>1</sub>                | 0.45     | 22.48                                  | 0.0021  | 0.21     | 6.05                                   | 0.0435  |
| X <sub>2</sub>                | 1.25E-03 | 0.062                                  | 0.8101  | 0.011    | 0.32                                   | 0.5881  |
| X <sub>3</sub>                | 0.13     | 6.23                                   | 0.0413  | 0.020    | 0.57                                   | 0.4739  |
| X <sub>1</sub> X <sub>2</sub> | 0.000    | 0.000                                  | 1.0000  | 2.5E-003 | 0.072                                  | 0.7968  |
| X <sub>1</sub> X <sub>3</sub> | 0.022    | 1.12                                   | 0.3249  | 0.01     | 0.29                                   | 0.6092  |
| X <sub>2</sub> X <sub>3</sub> | 0.72     | 36.00                                  | 0.0005  | 0.36     | 10.31                                  | 0.0148  |
| X <sub>1</sub> <sup>2</sup>   | 0.35     | 17.64                                  | 0.0040  | 0.70     | 20.02                                  | 0.0029  |
| X <sub>2</sub> <sup>2</sup>   | 1.47     | 73.02                                  | <0.0001 | 2.75     | 78.60                                  | <0.0001 |
| X <sub>3</sub> <sup>2</sup>   | 0.34     | 66.97                                  | <0.0001 | 0.34     | 9.62                                   | 0.0173  |
| Residual                      | 0.14     |  |         | 0.24     |  |         |
| Lack of fit                   | 0.033    | 0.40                                   | 0.7605  | 0.093    | 0.81                                   | 0.5503  |
| Pure error                    | 0.11     |  |         |          | 0.15                                   |         |
| Cor total                     | 4.96     |  |         | 4.98     |  |         |

\*The single seed rate model of the needle-type suction nozzle; <sup>o</sup>the single seed rate model of the plate-type suction nozzle.

dle-type suction nozzle reached the maximum value of 94.3%. Moreover, the optimal performance of the plate-type suction nozzle was obtained at the vacuum of 20.2 kPa, vibration frequency of 12 Hz, and seed suction height of 3.6 mm, which was 95.2%. The seeding tests were repeated to verify the accuracy of the models under the best parameter combination conditions of two suction nozzles, and the results showed that the actual seeding rate was 94.7% for the needle nozzle and 95.3% for the plate nozzle, which was very close to the model prediction values, and the reliability of the models was further verified. Figure 9 shows the seeding effect of the needle and plate nozzles.

From the above results, the needle suction nozzle requires a lower seed suction height and a lower vibration frequency than the plate suction nozzle; one reason might be that the needle has a small contact area with the grains, and lower suction height would effectively increase the probability of the needle clinging seeds. Another reason is that needle-type nozzle produces a more concentrated force on the grains, requiring less grain dispersion. The working characteristics of the plate-type nozzle are just on the opposite bank. The contact area between the plate nozzle and the grains is much larger, and the suction force of the suction holes is relatively dispersed, so the vibration frequency needs to be increased to reduce the adhesion force between the particles. As the vibration frequency increases, the vertical displacement of the seed increases, and the suction height increases accordingly.

To sum up, the needle-type nozzles absorb the seeds primarily through full contact with the grains, mainly reflected in lower seed suction height and less requirements for grain dispersion. In contrast, the plate-type nozzles require a larger vibration frequency to improve seed dispersion. Overall, the plate suction nozzle can

obtain better seeding performance, which is considered the more suitable choice for the vacuum-vibration tray precision seeder.

## Conclusions

In this paper, the stability and uniformity of airflow at the nozzles are improved by optimising the air chamber structure and discusses the seeding characteristics of the needle-type and plate-type suction nozzle on the vacuum-vibration tray precision seeder to obtain a more favourable nozzle structure. The main findings of the study are as follows:

- Based on the numerical simulation results, it was determined that higher air velocity and distribution uniformity could be achieved when the chamber height was 50 mm and the outlet tube diameter was 65 mm. Furthermore, the thickness of the base plate for plate-type suction nozzle should be less than 5 mm, while the length of the needle suction nozzle should be greater than 15 mm.
- The factors that significantly affected the seeding effect of both needle type and plate type nozzles were the same: vacuum, vibration frequency, and seed suction height, but the importance of each influencing factor and the influence effect on the two nozzles were different.
- The needle suction nozzle requires a lower suction height and less grain dispersion, while the plate suction nozzle requires more grain dispersion and allows for a certain suction height. Therefore, better seeding performance can be obtained using the plate suction nozzle, which is considered the more suitable choice for a vacuum-vibration tray precision seeder.

| Nomenclature             |  |                           |   |
|--------------------------|--|---------------------------|---|
| $A_1, A_2$               | the cross-sectional areas before and after the sudden change pipe, $m^2$   | $Pr_t$                    | Turbulent Prandtl number  |
| $C_{1e}, C_{2e}, C_{3e}$ | empirical constant   | $S_i, S_k, S_e$           | Source term   |
| $d$                      | pipe diameter, mm  | $u_i, u_j$                | mean of speed, m/s  |
| $f_N$                    | quadratic regression model between significant influencing factors and single grain rate of needle suction nozzle, % | $V$                       | mean velocity of pipe section, m/s  |
| $f_P$                    | quadratic regression model between significant influencing factors and single grain rate of plate suction nozzle, %  | $v_1, v_2$                | the velocities before and after the sudden change pipe, m/s                                   |
| $G_k$                    | generation term of the turbulent kinetic energy caused by average velocity gradient                                  | $Y_M$                     | contribution of pulsation expansion in compressible turbulence                                |
| $G_b$                    | generation term of the turbulent kinetic energy caused by buoyancy   | $Y_N$                     | linear model between influencing factors and single particle rate of needle suction nozzle, % |
| $h_f$                    | fractional loss, m   | $Y_P$                     | linear model between influencing factors and single particle rate of plate suction nozzle, %  |
| $h_{j1}$                 | the minor loss of sudden expansion pipe, m   | $\rho$                    | fluid density, $kg/m^3$   |
| $h_{j2}$                 | the minor loss of sudden contraction pipe, m   | $Re$                      | Reynolds number   |
| $k$                      | turbulent kinetic energy   | $\overline{\rho u_i u_j}$ | Reynolds stress term  |
| $l$                      | the length of pipe, m  | $\lambda$                 | on-way resistance coefficient   |
| $Ma$                     | Mach number  | $\mu$                     | hydrodynamic viscosity, Pa·s  |
| $p$                      | mean of pressure, Pa   | $\varepsilon$             | turbulent dissipation rate  |
|                          |  | $\beta$                   | coefficient of the thermal expansion  |

## References

- Bernardi C., Dib S., Girault V., Hecht F.F.M., Sayah T. 2018. Finite element methods for Darcy's problem coupled with the heat equation. *Numer. Math.* 2:315-48.
- Du R., Liu Z., Jiao Y., Meng W. 2017. Flow field simulation test and optimization of plate of tray seeder[J]. *J. Agric. Mechan. Res.* 7:148-152.
- Gaikwad B.B., Sirohi N.P.S. 2008. Design of a low-cost pneumatic seeder for nursery plug trays. *Biosyst. Engine.* 99:322-9.
- Gao X., Zhang Z. 2016. The analysis and study on air flow field of air suction metering device for 2BQM-2 seeder. *J. Agric. Mechan. Res.* 38:66-70+88.
- Gunst R.F., Myers R.H., Montgomery D.C. 1996. Response surface methodology: process and product optimization using designed experiments | *Clc. Technometrics.* 38:203-37.
- Han Z., Wang G. 2016. Fundamental engineering fluid mechanics. J. Beijing Inst. Technol. pp. 71-97.
- Hassan Y.S., Liao Q. 2014. Simulation of negative pressure behavior using different shapes and positions of pressure inlet and seed hole diameters using ANSYS-CFX to optimize the structure of a pneumatic metering device designed for wheat. *Agric. Engine. Int. Cigr J.* 16:122-33.
- Krishnasreni S.P.T. 2004. Status and trend of farm mechanization in Thailand. *Agric. Mechan. Asia Afr. Latin Am.* 1:59-66.
- Liao Y., Zheng J., Liao Q., Ding Y., Gao L. 2019. Design and experiment of positive and negative pressure combined tube - needle centralized seeding device for American ginseng. *Trans. Chinese Society Agric. Machin.* 050:46-57.
- Liu C., Song J., Wang J., Wang C. 2010. Analysis of flow field simulation on vacuum seed-metering components of precision metering device with sucker. *J. China Agric. Univ.* 15:116-20.
- Liu J., Wang Q., Li H., He J., Lu C., Wang C. 2020. Numerical analysis and experiment on pneumatic loss characteristic of pinhole-tube wheat uniform seeding mechanism. *Trans. Chinese Soc. Agric. Machin.* 51:36-44.
- Liu Y., Zhao M., Liu F., Yang T., Zhang T., Li F. 2016. Simulation and optimization of working parameters of air suction metering device based on discrete element. *Trans. Chinese Soc. Agric. Machin.* 047:65-72.
- Montgomery D.C. 2019. Design and analysis of experiments. Post and Telecommunications Press, pp. 349-354.
- Tiw-An C., Gavino R., Gavino H., Lavarias J. 2020. Development of a seeding tray seeder for lettuce (*Lactuca sativa* L.) production. *E3S Web of Conf.* 187:05002.
- Versteeg H.K., Malalasekera W. 1995. An introduction to computational fluid dynamics: the finite volume method. New York: Wiley.
- Wang F. 2004. Computational fluid dynamics analysis. Beijing: Tsinghua University Press.
- Xia H., Li Z., Niu J., Lin X. 2008. Dynamic model for metering process for pneumatic roller-type vegetable seeder. *Trans. CSAE* 24:141-6.
- Yasir S.H., Liao Q. 2014. Simulation of negative pressure behavior using different shapes and positions of pressure inlet and seed hole diameters using ANSYS-CFX to optimize the structure of a pneumatic metering device designed for wheat. *Agric. Engine. Intern. Cigr J.* 16:122-34.
- Yazgi A., Degirmencioglu A. 2014. Measurement of seed spacing uniformity performance of a precision metering unit as function of the number of holes on vacuum plate. *Measurement* 56:128-35.
- Zhao Z., Tian C., Wu Y., Huang H. 2018. Dynamic simulation of seed pick-up process and parameter optimization on vacuum plate seeder for rice. *Trans. Chinese Soc. Agric. Engine.* 34:38-44.
- Zhao Z., Wang J., Liu L., Liu Z., Wang W. 2015. Advance research of tray precision sowing equipment. *J. Agric. Mechan. Res.* 000:1-5, 25.